Available online at www.sciencedirect.com
SCIENCE DIRECT
Polymer 46 (2005) 6595–6604
polymer
www.elsevier.com/locate/polymer

Effect of composition of added random copolymer on the phase behavior of block copolymer

Dae-Cheol Kim, Seong Il Yoo, Sik-Won Moon, Wang-Cheol Zin*

Department of Materials Science and Engineering, Pohang University of Science and Technology, Pohang 790-784, South Korea

Available online 23 May 2005

Abstract

Blends of styrene–butadiene diblock copolymer (S–B, 52 wt% styrene content) and styrene–butadiene random copolymer (SBR) of various styrene compositions were studied by small-angle X-ray scattering, light scattering, and transmission electron microscopy. The composition of random copolymer plays an important role in the solubilization of SBR in S–B. The order–disorder transition temperature, T_{ODT}, decreases linearly with the addition of SBR. T_{ODT} decreases as the symmetry in SBR composition increases and shows the highest value in the case of homopolymers. Asymmetric butadiene-rich SBR dissolves mostly into PB microdomain of S–B to increase lamella microdomain spacing, D, and its addition makes the overall microdomains of S and B in the mixture more asymmetrical. Symmetric SBR is localized into the interface of S–B microdomain to reduce unfavorable S–B contact at the interface. The phase diagram for S–B containing asymmetric SBR shows a succession of mixed mesophases of different morphologies from lamellae and cylinder to disordered liquid phases, whereas the phase diagram containing symmetric SBR shows two homogeneous phases and one region of two-phase coexistence, where macroscopically separated phases coexist together.

Keywords: Block copolymer; Random copolymer; Phase diagram

1. Introduction

Many studies have investigated the phase behavior in binary mixtures of diblock copolymer and homopolymer [1–14]. Nojima and Roe undertook studies on diblock copolymer (A–B)/homopolymer (A) blend [7], and showed (1) that, when a small amount of A is dissolved into A–B, the spinodal temperature (T_S) is either elevated or lowered according to the molecular weight ratio of A over A–B, (2) so that the magnitude in the change of T_S is higher with larger amounts of added homopolymer. Tanaka and Hashimoto [15] studied order–disorder transition temperature, T_{ODT}, of styrene–isoprene diblock copolymer on addition of polystyrene and DOP (dioctyl phthalate, neutral solvent) in a regime where PS is solubilized in styrene microdomains. Solvent DOP is most effective in lowering T_{ODT}, and the degree of depression is slowed by increasing the molecular weight of PS. This tendency is in good agreement with that predicted by Noolandi et a1. [5]. There have also been some studies [16–20] on block copolymer/block copolymer blends, or block copolymer/random copolymer blends, which are expected to exhibit different phase behavior from diblock copolymer/homopolymer blends.

In addition to the above studies, an extension to diblock copolymer solutions with a neutral (nonselective) solvent has been carried out [21–25]. A theory developed by Whitmore and Noolandi [26] predicted that, if the solvent is a good solvent of roughly equal affinity for both of the blocks, the copolymer solution will display thermodynamics similar to that of the pure melt and there will be a tendency for neutral solvents to accumulate at the microdomain interface to screen unfavorable A–B monomer contacts at the interface. Lodge et al. [25] constructed a phase diagram for styrene–isoprene diblock copolymers by varying the selectivity of added solvents. Each solvent became less selective as T increased, inducing a variety of thermally accessible order–order transitions (OOTs) such as lamella, cylinder, and spherical micelles. The addition of a neutral solvent is analogous to increasing temperature or reducing effective interaction parameters, and the principal interdomain distance decreases as solvent the volume

* Corresponding author. Tel.: +82 54 279 2136; fax: +82 54 279 2399.
E-mail address: wczin@postech.ac.kr (W.-C. Zin).

0032-3861/$ - see front matter © 2005 Elsevier Ltd. All rights reserved.
doi:10.1016/j.polymer.2005.05.013

fraction increases. In one of our previous studies [18], we constructed a theoretical phase diagram for diblock copolymer (A–B) blends containing random copolymers (ABR) with compositions similar to those of diblock copolymers. The T_{ODT} of block copolymers was lowered by the addition of random copolymers regardless of their molecular weight. It was also found that the fraction of ABR solubilized into the A–B was very limited due to endothermic mixing between ABR and each block of A–B. An experimental study [19,20] on A–B/ABR blends was subsequently carried out, where the composition and molecular weight of ABR were similar to those of A–B. We showed that the T_{ODT} and the interdomain distance (D) almost linearly decreased as the ABR fraction increased within the solubility limit.

In the present study, binary blends containing symmetric diblock copolymer (A–B) and random copolymer (ABR) of various compositions are studied by small angle X-ray scattering (SAXS), light scattering (LS), differential scanning calorimetry (DSC), and transmission electron microscopy (TEM) techniques. AB random copolymer was chosen as the diluent, and the effect of composition of added random copolymer on the phase behavior of A–B is discussed. It is expected that, at temperatures below the T_{ODT} where A–B has a lamellar morphology, ABR will have solubility to A–B depending on the styrene composition of ABR: (1) if added ABR has asymmetric composition, it will dissolve either at the A or B domain of A–B to extend lamella microdomain thickness, and (2) if added ABR has symmetric composition, it will have poor solubility to both A and B domains and may dissolve at the interface of the microdomains to reduce unfavorable interaction between ABR and A-, B-monomers of A–B ($\chi_{ABR/PA} \approx \chi_{ABR/PB} \approx 0.5\chi_{A/B}$). Macroscopic phase separation will occur above the solubility limit of SBR, which will be evidenced by optical turbidity in LS and TEM experiments. Block copolymer-rich mesophase may still reveal a periodic peak profile in SAXS and heat change of microdomain formation in DSC experiments, since this is in a similar state to pure block copolymers. These independent experiments were carried out to give complementary results on the phase behavior of A–B/ABR blends, and an experimental phase diagram will be constructed.

2. Experimental section

2.1. Materials

The information of the copolymers used is listed in Table 1. Styrene–butadiene diblock copolymer (denoted by S–B50) is the same material used in the previous study [19,20], which contains 52 wt% of styrene as determined by the NMR technique, and its M_n and M_w are 25,000 and 26,000, respectively. The blend samples were prepared by first dissolving a predetermined amount of each copolymer in toluene in the presence of an antioxidant (Irganox 1010, Ciba–Geigy Group) and then by slow evaporation of the solvent at room temperature. To remove the residual solvent, the samples were further dried under a vacuum at about 60 °C for over a day. After complete removal of the solvent, the samples were further annealed at 120 °C for 24 h. The mixture sample was designated by the sample label followed by their weight percentages, as in 'SB50/SBR50 (90/10)'.

2.2. Methods

Synchrotron small-angle X-ray scattering (SAXS) measurement was performed at the 4C1 and 4C2 X-ray Beamline (1.608 Å in wavelength) at the Pohang Accelerator Laboratory (PLS) in Korea. The beam path was maintained under a vacuum to reduce air scattering, and the measured intensity was corrected for ring current decrease, background scattering, detector noise, and sample absorption. Since the optics of the SAXS equipment are point focused, the intensity was not corrected for the smearing effect by the primary beam. The heating and cooling rate was fixed at 2 °C/min, and the data were collected every 5 °C between room temperature and the experimental limit. Since reproducibility was shown between the heating and cooling results, we mainly used the cooling data in the present study.

The cloud temperature was determined from light scattering (LS) experiments by monitoring the intensity of scattered light at a fixed angle ($\sim 30°$) through a mixture film located on a heating stage. A He–Ne laser (4 mW) was used as a light source. Heating and cooling experiments were performed several times to increase the validity of the experimental results. The same heating system was used as in the SAXS experiments, which made it possible to compare the two independent data sets directly without any further corrections between them.

Thermal analysis was performed with a Perkin–Elmer DSC7. T_{ODT} was determined from the change of exothermic enthalpy during the cooling scan. Each sample was heated far above the melt state and then cooled to room temperature at the rate of −10 °C/min. Glass transition temperatures were measured during reheating at a rate of 20 °C/min after the samples had been held at 150 °C and then cooled to −150 °C at −20 °C/min.

The transmission electron microscopy (TEM) samples were prepared by placing a drop of solution on a carbon-/Formvar-coated copper grid and letting the solvent evaporate at room temperature on a sealed glass vessel. To remove the solvent evaporation effect that could have affected the observed morphology of solution-cast block copolymers, the solvent was very slowly evaporated and the samples were annealed at 35 °C for a day. To attain equilibrium morphology, the samples were further annealed above the glass transition temperatures of both blocks in a vacuum oven for 5 h. The samples were then exposed to the

Table 1
Characteristics of copolymers used in this study

Brief	Copolymer	Composition (wt% styrene)[a]	Molecular weight	
			M_w[b]	M_w/M_n[c]
S–B50[d]	Poly(styrene-*b*-butadiene)	52	26,000	1.04
SBR00[d]	Polybutadiene	0	26,000	1.04
SBR25[d]	Poly(styrene-*r*-butadiene)	25	24,000	1.07
SBR50[d]	Poly(styrene-*r*-butadiene)	50	24,000	<1.10
SBR60[e]	Poly(styrene-*r*-butadiene)	60	50,000	1.07

[a] Obtained from ^{1}H NMR.
[b] Obtained from LS.
[c] Obtained from GPC.
[d] Synthesized by Dr H.L. Hsieh of Phillips Petroleum Co.
[e] Synthesized by Kumho Chemical Co.

vapor of a 2% aqueous OsO_4 solution, a selective staining agent for the butadiene blocks. TEM was performed on a JEOL 1200EX electron microscope operated at 120 kV.

3. Results and discussion

3.1. Determination of order–disorder transition temperatures

The microscopic phase behavior of the mixture was examined using the SAXS technique to investigate the effect of added SBR on the stabilization of S–B50 microdomain structure. Scattered X-ray intensity data were obtained with S–B50/SBR having various SBR weight fractions. From the plot of the scattered X-ray intensity against the scattering vector q at room temperature, first, third, and fifth Bragg peaks for S–B50 appeared at $q=0.29$, 0.88, and 1.47 nm^{-1}, respectively. Thus, the ordered morphology of S–B50 is lamellar as evidenced by the peak scattering vector ratios. The first peak ($D=2\pi/q^*$) corresponds to a lamellar interdomain spacing of 22.5 nm. Based on the discontinuity in the plot of $S^{-1}(q^*)$ vs. T^{-1}, the T_{ODT} of S–B50 was found to be 186 °C (459 K).

Fig. 1 shows the X-ray scattering intensities obtained with three blend samples containing various concentrations of SBR at 323 K. As for S–B50/SBR00, the higher order peaks for each sample occur at q values which are exact multiples of the firstorder peak, indicating that the morphology is lamellae. With neat S–B50, the even-order peaks are almost absent, reflecting block domain symmetry. As the SBR00 increases, the peak positions shift toward smaller angles, showing that the lamellar interdomain spacing increases. At the same time, the relative heights of the peaks change. The butadiene layer becomes thicker than the styrene layer which causes the relative heights of even vs. odd peaks to change. With S–B50/SBR25 samples, the trend with increasing SBR is similar to S–B50/SBR00. In the case of S–B50/SBR50, the positions of first-order peaks are almost identical, and no second order peak appears. This indicates that S–B50/SBR50 samples form symmetric lamellar microdomains of equal size, and therefore, that the added SBR50 barely dissolves into the S–B50 microdomains. As SBR50 increases, the peak width is broadened and the intensity is lowered, indicating that mixtures containing higher SBR50 have less long-range order. With S–B50/SBR60 samples, a similar trend to S–B50/SBR50 was observed.

Fig. 2(a) displays the scattered primary X-ray intensity profiles of S–B50/SBR60 (80/20) near the T_{ODT} on cooling. A sharp change of the profiles at temperatures between 399 and 413 K is clearly observed. The T_{ODT} can be determined from this discontinuous change in the SAXS profile [15,27]. The narrow peak obtained below the T_{ODT} is the first Bragg reflection of the lamellar microdomain periodic structure. After an abrupt intensity drop at 413 K, the intensity is continuously reduced by raising the temperature. The remnants of the peaks that persist to the highest temperature are due to the concentration inhomogeneity present even in a thermodynamically homogeneous polymer melt, stemming from the so-called correlation hole effect [28]. Repulsive interactions between styrene and butadiene drive local physical clustering of similar segments, and this process results in a finite size stabilization of the disordered state on the microdomain length scale [29]. Fig. 2(b) shows the three plots of I_m^{-1} vs. T^{-1}, σ^2 vs. T^{-1}, and D vs. T all together for S–B50/SBR60 (80/20) on cooling. Here, I_m indicates the maximum intensity of the primary peak and σ^2 the square of the half-width at halfmaximum of the primary peak. D is determined from the scattering vector q^* at the first-order scattering maximum. It is clearly seen that the abrupt increase in σ^2 or I_m^{-1} with decreasing T^{-1} occurs almost at the same temperature. The steady diminution of D upon increasing T corresponds to the shift of the peak position toward higher q value in Fig. 1(a), which is due to chain shrinkage of a Gaussian coil arising from an increase in entropy on mixing. We observed that D increases slightly upon raising the temperature across T_{ODT}, and that this discontinuity in D is expected since ODT is a weak first-order transition [30]. In a disordered state, D corresponds to the spatial extent of concentration fluctuations, which are activated by thermal energy, whereas in

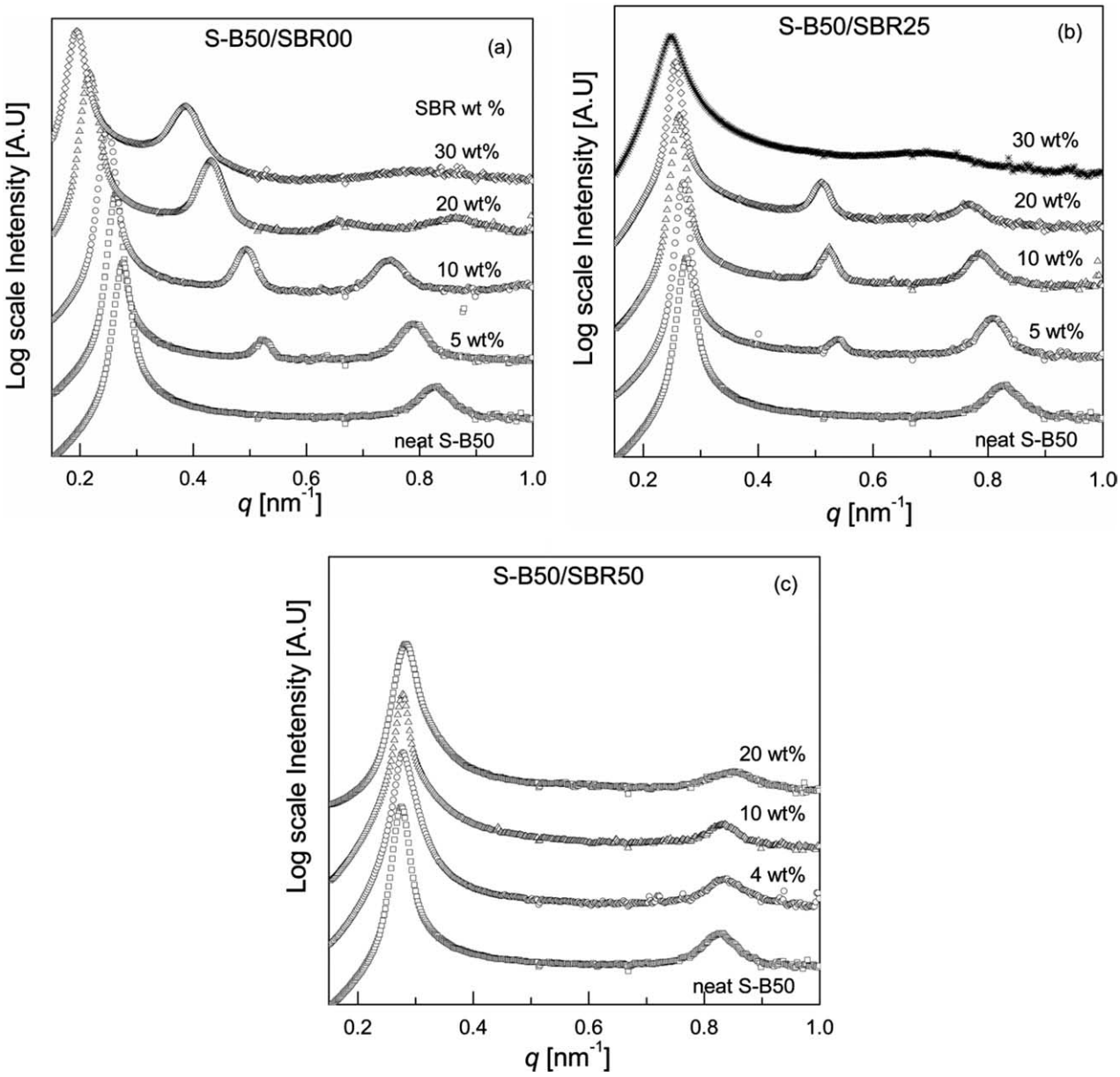

Fig. 1. SAXS profiles from three blends containing various amounts of SBR at 323 K: (a) S–B50/SBR00, (b) S–B50/SBR25, and (c) S–B50/SBR50. Curves are shifted vertically for clarity.

the ordered state, it corresponds to the spacing for lamellar microdomain structures generated by block segregation. As for other mixtures, a similar plot to Fig. 1(b) is obtained.

The T_{ODT}'s obtained for S–B50 containing SBR with various styrene composition are summarized in Fig. 3, and compared each other to verify the effect of the composition of added random copolymer. T_{ODT} decreases linearly on the addition of SBR, indicating that dissolved random copolymer stabilizes disordered phase more than lamella mesophase. When SBR00 (butadiene homopolymer) is added to S–B50, T_{ODT} shows a slight depression. SBR00 dissolves preferentially into the PB microdomain of S–B50 and its addition makes the overall composition of S and B in the mixture more asymmetrical. When a small amount of homopolymer A is dissolved into A–B, T_{ODT} is either elevated or lowered according to the molecular weight ratio of A over A–B, and that T_{ODT} change is greater with larger amounts of added homopolymer [7]. As shown in Fig. 3, in the case of homopolymer (SBR00) having a similar molecular weight to SB50, T_{ODT} is almost unchanged. On the other hand, when SBR having symmetric composition (SBR50) is added to S–B50, T_{ODT} decreases faster because SBR acts as a neutral solvent. When SBR50 is mixed with melt S–B50 having no microdomains, they can be mixed homogeneously with favorable enthalpy change ($\Delta H = 0$) and an increase in mixing entropy. Therefore, disordered liquid phase becomes thermodynamically stable, and T_{ODT} decreases. When the reduction of T_{ODT} is compared with

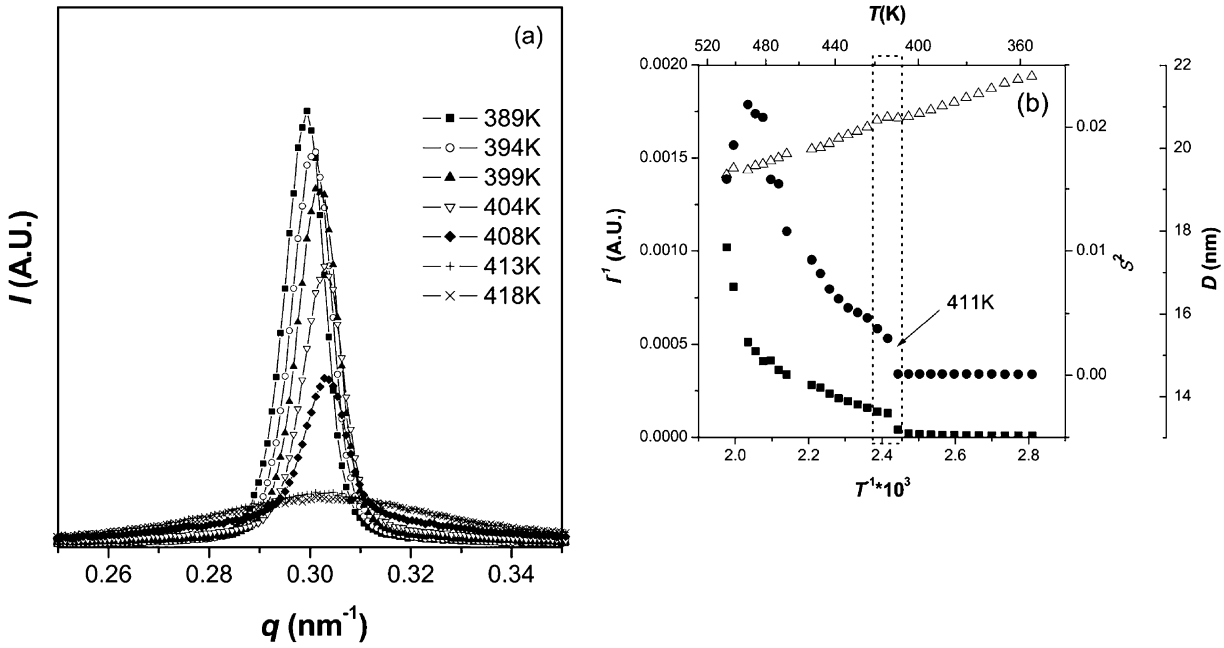

Fig. 2. (a) SAXS intensity of S–B50/SBR60 (80/20) as a function of temperature. T_{ODT}=411 K, after which a sharp decrease in intensity is seen with increasing temperature. (b) Plots of I_m^{-1} (■) vs. T^{-1}, σ^2 (●) vs. T^{-1}, and D (△) vs. T. The discontinuity of each plot appears at the same temperature marked by the dotted box (411 K).

dilution approximation (solid line) [26], S–B50/SBR50 shows a very similar trend. As will be discussed later, SBR50 or SBR60 is not completely homogeneously mixed as dilution approximation assumes, but might be localized into the interface of S–B50 microdomain.

3.2. Solubilization of SBR into S–B microdomains

When a diluent is dissolved in the lamella microdomain of block copolymer, lamella domain spacings vary differently depending on the location of added diluent. Hashimoto et al. [8] described the change of lamella domain spacings on addition of homopolymer according to whether the swelling involves localized or uniform solubilization. Added homopolymers will mostly dissolve into A-domain if they have selectivity to A, extending A-domains. However, the degree of extension depends on the location of added homopolymers. If homopolymers are localized at the center of microdomains, it will extend the domain at direction vertical to the interface. The expansion of D/D_0 is related to the change of the interfacial density of the chemical junctions ρ_j/ρ_{j0}.

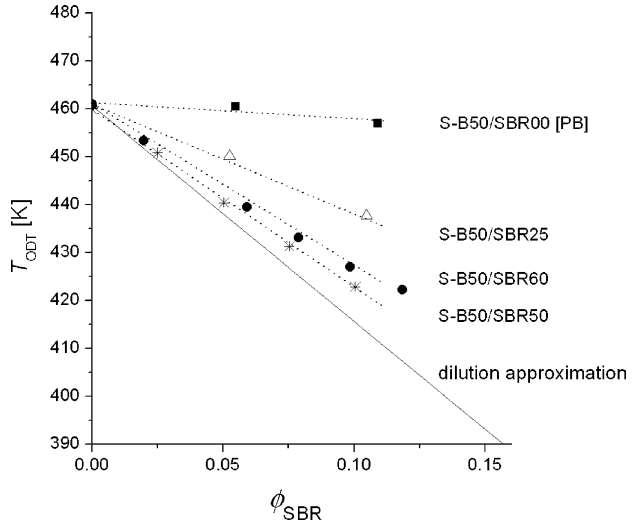

Fig. 3. The T_{ODT}'s obtained from SAXS results are plotted against SBR weight fraction. The dotted lines are drawn as a guide to the eye, and the solid line is calculated T_{ODT} from dilution approximation.

$$\frac{D}{D_0} = \frac{\rho_j}{\rho_{j0}(1-\phi)} \tag{1}$$

for the alternating lamellar microdomains where ϕ is the volume fraction of the homopolymers in the mixture. The localized solubilization of the homopolymers as an extreme gives $\rho_j/\rho_{j0}=1$. In contrast, if homopolymers are uniformly solubilized throughout one microdomain, they will also extend the distance between the junction points at the interface, resulting in domain extension parallel to the interface. The expansion of D/D_0 for the binary mixtures of A–B/B as a function of the volume fraction of homopolymer can be expressed as

$$\frac{D}{D_0} = \frac{1}{[(1-\phi)(1+\phi^2)]^{1/3}} \tag{2}$$

Fig. 4 shows lamella domain spacing, D, for blends normalized to that of a neat block copolymer, D_0, as a function of the fraction of random copolymer. D was obtained experimentally from the peak position of first order

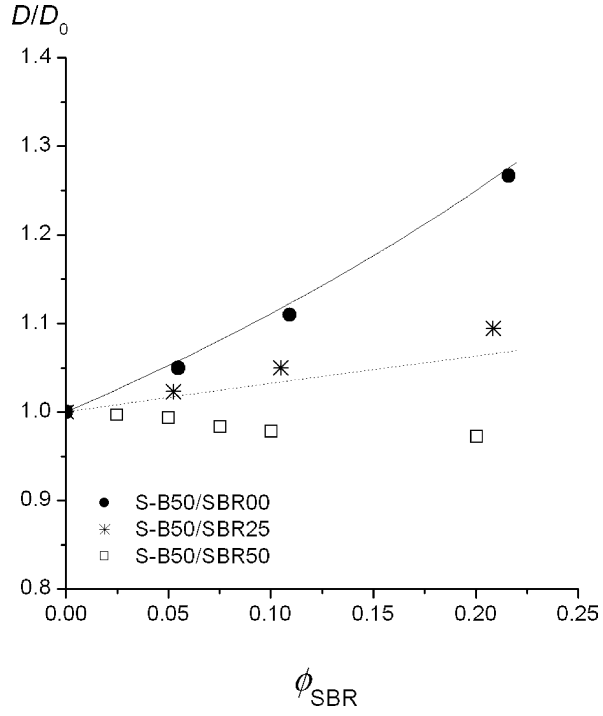

Fig. 4. Lamella domain spacing, D, for blends normalized to that of a neat block copolymer, D_0, as a function of the fraction of random copolymer. Scattered data denote experimentally obtained D/D_0 from the SAXS first order peak position. The solid and dotted lines are calculated according to lamellar solubilization models.

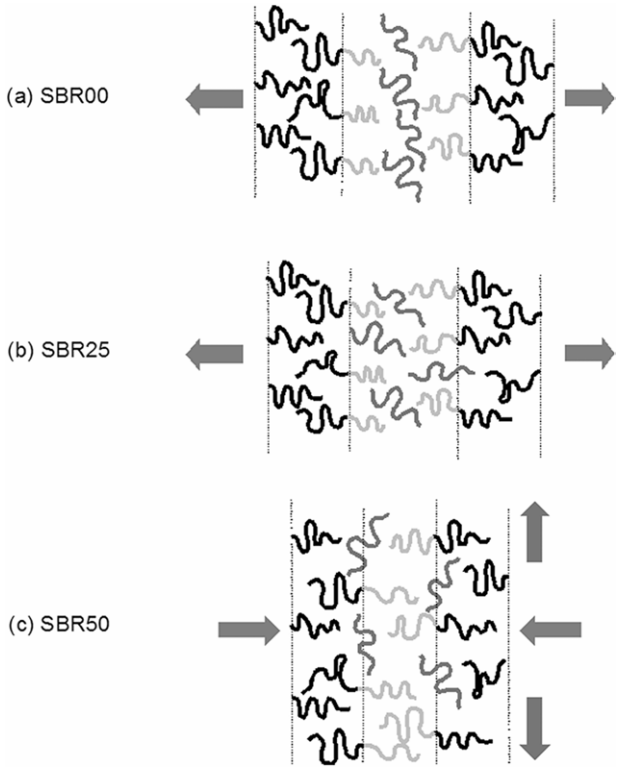

Fig. 5. Schematic representation of lamella domain spacing, D, of S–B50 on addition of SBR. SBR25 dissolves selectively at PB domains whereas SBR50 dissolves at the interfacial region of S–B50 microdomains.

maximum at a temperature slightly above the glass transition temperature. It is seen that D gradually increases as the fraction of SBR00 increases. Since SBR00 mostly dissolves into the PB domain of S–B50 and is localized at the center of PB domains, the measured lamella microdomain distance is extended vertical to the interface. In contrast, when SBR50 is added into SB50 lamellar microdomains, D slightly decreases on addition of SBR50. Surmising from the selectivity of SBR50, it can be deduced that SBR50 does not dissolve to either of S or B domains, instead it dissolves at the interfacial region. On this assumption, added SBR50 can significantly extend the junction point, resulting in domain extension at a direction parallel to the interface. Thus it lowers the distance D, which is the distance vertical to lamella interface. The solid line is calculated for localized solubilization of the homopolymers as an extreme, and the dotted line is the one for uniform solubilization [31]. It is obvious from this figure that SBR25 in the blends must be distributed in microdomains in the intermediate states of the two extreme cases described above. This estimation is well described in Fig. 5, which shows a schematic representation of the S–B50 lamella domain on addition of SBR. It should be noted that SBR50 solubilization at the interface of S–B50 (c) can decreases D further than any models described above. For a detailed investigation of the location of SBR in the microdomain structure of block copolymer, the small-angle neutron scattering (SANS) technique can be utilized as suggested by Matsushita [31] and Lodge [24] et al.

3.3. Macroscopic phase separation and morphology evolution

The electron micrographs of blends containing 10 and 20 wt% of SBR60 are shown in Fig. 6(a) and (b). A blend containing 10 wt% of SBR60 forms S–B50 lamellar microdomain structures mixed with a small amount of SBR60, and blend containing 20 wt% of SBR60 forms both lamellar microdomains and macroscopically phase-separated domains of SBR60. Lamellar microdomains rich in S–B50 are composed of alternating lamellae of styrene and butadiene microdomains corresponding to the equilibrium morphology of neat S–B50. Butadiene domains appear dark and styrene domains bright in the lamellar microphase of blends in the TEM micrograph due to selective staining. With blend exhibiting a solubility limit, SBR60 rich macrophase dispersed within the matrix of block copolymer phase develops. Also, lamella structures in the matrix phase are retained but are disturbed to induce disordering of the lamellar order. As shown in Fig. 6(b), the ordered 'M' phase rich in S–B50 and the disordered 'L' phase rich in SBR60 coexist in a macroscopically phase separated 'M + L'. Fig. 7 shows the electron micrograph of S–B50 blends containing SBR25, and we can observe much wider variations of

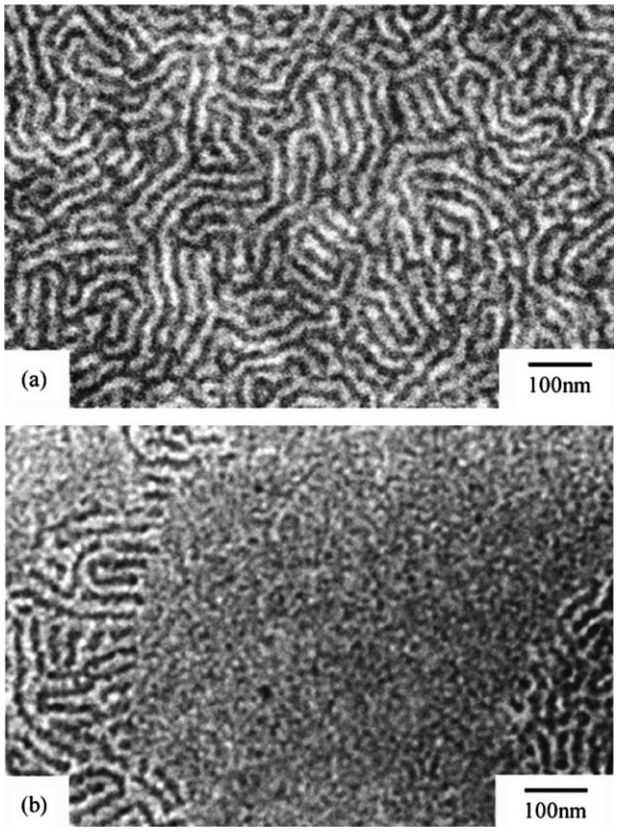

Fig. 6. TEM images of S–B50/SBR60 blends at various SBR concentrations: (a) blend containing 10 wt% SBR, (b) blend containing 20 wt% SBR. Butadiene blocks were selectively stained with OsO_4 and appear as dark regions.

morphological features as SBR25 weight fraction increases. At 20 wt% SBR25 (a), lamellar structure is still maintained, but it seems that there is also, cylinder phase mixed with lamellae. This becomes more evident at 35 wt% SBR25 (b), where the lamellar order is changed into disordered cylinder phase. At 50 wt% (c), an irregular disconnected network of cylinder phase mixed with disordered liquid phase is seen, which on further dilution with SBR25, at (d), turns into what appear to be cylindrical random micelles dispersed in disordered liquid. With blends having 20–30 wt% SBR25, cylindrical phase with hexagonal order has not yet been observed.

3.4. Phase diagrams

In Fig. 8, the transition temperatures obtained with the SAXS, LS, and DSC experiments are plotted as a function of the weight fraction of SBR50 and SBR60 [19,20]. The 'L' phase above the transition line indicates the homogeneous mixed phase of S–B50 and SBR in a disordered state. The 'M' phase below the transition line indicates the ordered microdomain structure of S–B50 mixed with SBR. The T_{ODT} shows a two-step dependency on the weight fraction of SBR: in the region where the SBR weight fraction is lower than 0.15, the T_{ODT} shows a linear depression which can be compared with that from dilution approximation. The T_{ODT} is determined by comparing the free energy changes between solubilized lamellae and mixed liquid phases. A macroscopic phase separation from 'M' to 'M+L' occurs above the solubility limit, and the T_{ODT} above the solubility limit shows little dependency on the SBR weight fraction. We note that the results of the LS experiments show a good correspondence with those of the SAXS experiments. In the region where the SBR weight fraction is larger than 0.7, there is a very small amount of 'M' phase in this region, resulting in the disappearance of the Bragg reflection peaks in the SAXS experiments. Thus, we cannot investigate the order–disorder transition by using the SAXS method. As seen in Fig. 8, however, by using the LS method, the macroscopic phase separation transition between 'L' and 'M+L' phases can be examined in this region. This means that a macroscopically phase-separated state, 'M+L', remains below that transition line, even though the S–B50-rich phase loses its long-range order.

The depression of the T_{ODT} in the region where the SBR weight fraction is larger than 0.15 may be understood by considering the melting point depression occurring in crystalline polymer/good solvent systems. The ordered phase is comprised of S–B50 microstructures mixed with a small amount of SBR in the interface, and the disordered phase is comprised of SBR containing a small amount of S–B50. There are two differences between S–B50/SBR50 (SBR60) and common crystal/solvent systems: (1) an increase in mixing entropy of added random copolymer is less than that of added solvent, and (2) there is slight random copolymer solubilization in the formation of mesophase. It should be noted that SBR has poor solubility to either the S- or B-domain of S–B50.

To explain the drop of the T_{ODT} above the solubility limit, the free energy change of the mesophase 'M' can be compared to that of disordered liquid phase 'L' at various temperatures. In one of our previous studies [18], a theoretical phase diagram was constructed for S–B blends containing SBR with compositions similar to those of diblock copolymer which are shown as solid (SBR50) and dotted (SBR60) lines in Fig. 9(a). The parameters used for S–B50/SBR50 and S–B50/SBR60 blends in this figure are as follows: interaction energy density $B_{S/B}=1.6–0.002T$ (cal/cm^3), $M_{S–B}=25000$, $M_{SBR}=46730$, $f_S=0.52$, $f'_S=0.5$ and 0.6. Since the theory assumed a sharp interface boundary, solubilization of SBR at the interface was not considered. SBR is barely dissolved into the microdomain of S–B50 due to the increased mixing enthalpy, that is, macroscopic phase separation occurs when the SBR is added to S–B50. The phase boundary between 'M' and 'M+L' is not displayed since mesophase M exists only over a narrow concentration range of ϕ_{ABR} near $\phi_{ABR}=0$ for temperatures below the T_{ODT} of pure S–B50. The mixture of $f'_S=0.5$ shows a lower T_{ODT} than that of $f'_S=0.6$ due to the decrease in the enthalpy energy change of liquid phase. However, if we consider the solubilization of random

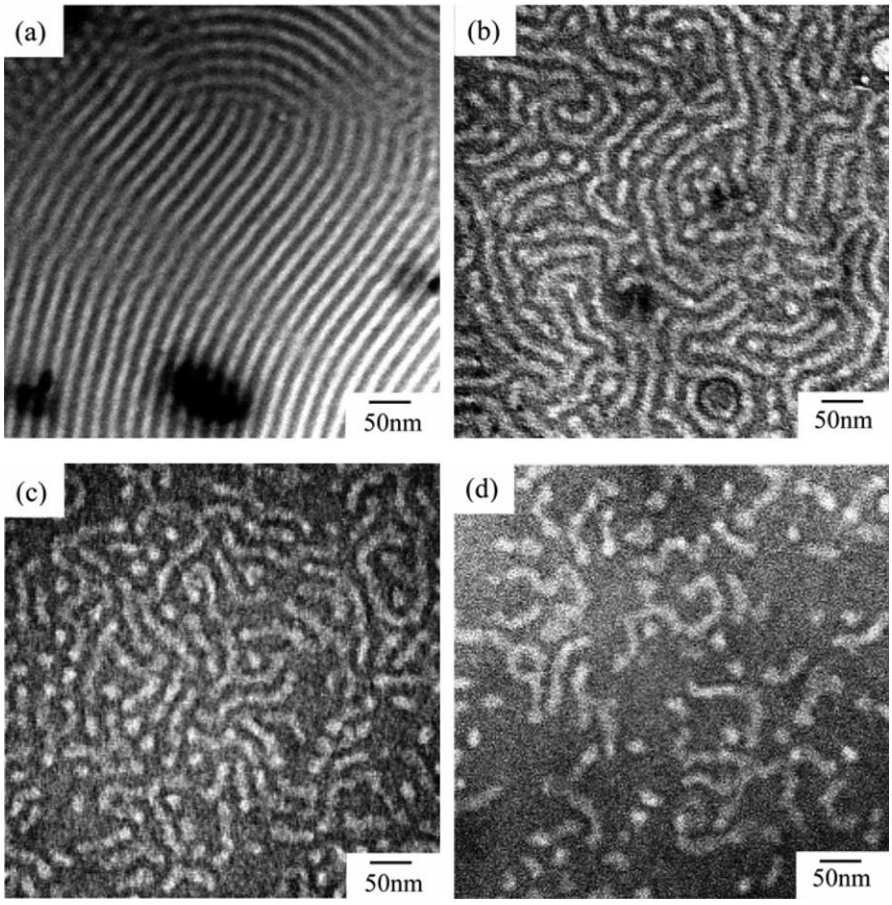

Fig. 7. TEM images of S–B50/SBR25 blends at various SBR concentrations: (a) blend containing 20 wt% SBR, (b) 35 wt% SBR, (c) 50 wt% SBR, and (d) 60 wt% SBR.

copolymer in the interfacial regions in microdomains as figured by the gradual reduction of D below the weight fraction of 0.15, the increase in enthalpic energy on solubilization will be negligible since the compositions of SBR50 or SBR60 are very close to that in the interfacial region. The phase diagram, considering the possibility of solubilization of random copolymer in the interfacial region, is shown as a dashed line in Fig. 9(b). However, there is a difference between SBR50 and SBR60. As discussed earlier, T_{ODT} of S–B50 containing SBR50, having symmetric styrene composition, decreases faster than that containing SBR60. Therefore, even though the solubility limit of both SBR50 and SBR60 is similar, SB50/SBR50 has lower T^*_{ODT}, at which macroscopic phase separation occurs ($\sim$15%). The T_{ODT}'s for both blends then decreases steadily following the same depression trend upon the mixing of melt 'M' phase with 'L' phase.

The constructed phase diagram for S–B50/SBR25 is shown in Fig. 10. The 'L' phase above the transition line indicates the homogeneous mixed phase of S–B50 and SBR25 in the disordered state. The 'M_1' phase indicates the ordered lamella structure of S–B50 mixed with SBR, and the 'M_2' phase indicates a cylindrical structure. The T_{ODT} shows a prominent depression after which the T_{ODT} shows little dependency. A mixed transition between order–order transition and macroscopic phase separation transition can be seen. With these systems a succession of mixed mesophases of different morphologies appears between M_1 and L phases as Fig. 10 shows. 'M_1' essentially remains as a single lamella phase within a solubility limit of SBR25. The macrophases that separate out beyond the solubility limit would be a mixture of 'M_1' and another mesophase 'M_2', and then 'M_1' gradually disappears. As the concentration of SBR increases, SBR25 rich disordered liquid phase 'L' separates out to form a mixed macroscopic phase of 'M_2' and 'L'. The T_{ODT}'s of S–B50 containing 20–30 wt% SBR25 could not be determined because the SAXS profiles of blend samples did not show a sharp T_{ODT}, but rather showed continuous transitions from ordered to disordered states. We believe, on the basis of the following observations that this kind of mixed transition stems from a possible non-equilibrium state since the transition temperature lies in the vicinity of the styrene blocks glass transition temperature. In addition, unlike A–B/H (homopolymer) systems which show discrete order–order transitions, added SBR25 may have weak selectivity to either S- or B-domains, and the driving force to form a definite morphology is not strong.

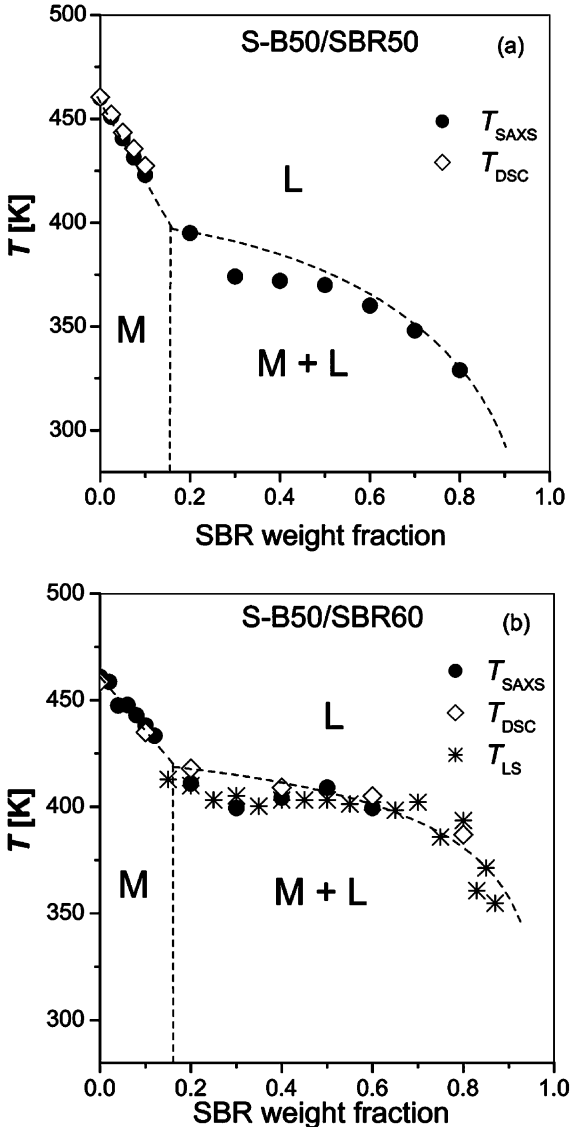

Fig. 8. Phase diagram obtained from the SAXS, DSC, and LS studies for (a) SB50/SBR50 and for (b) S–B50/SBR60. Listed symbols are T_{SAXS} (●), T_{LS} (∗), and T_{DSC} (◇). These independent experiments show good agreement with each other. The dashed line denotes the phase boundary from 'M+L' to 'L' and that from 'M' to 'M+L' drawn as a guide to the eye.

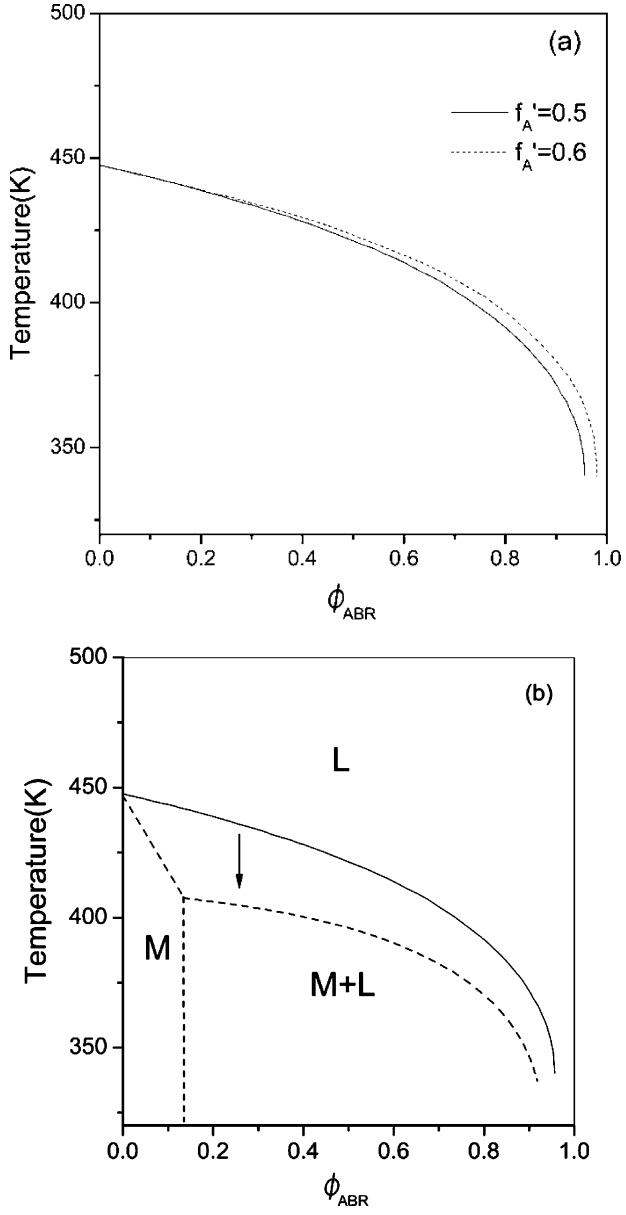

Fig. 9. (a) The effect of component A of the ABR, f'_A, on the phase behavior of the AB/ABR blends, in which only the transition from 'M+L' phase to 'L' phase is highlighted. The solid line denotes the result of f'_A= 0.5 and the dashed line the result of f'_A=0.6. (b) The schematic phase diagram for A–B/ABR, considering the possibility of solubilization of random copolymer in the interfacial region, is plotted as the dashed line. The solid line is a calculated phase boundary from (a).

4. Conclusion

From the SAXS study, the order–disorder transition was examined on S–B diblock copolymer containing SBR random copolymers. Attention was focused on the composition effect of the added random copolymer on T_{ODT} depression and the change of D for A–B/ABR binary blends. T_{ODT} was found to decrease gradually on the addition of SBR. When SBR with asymmetric composition (SBR25) is added to S–B50 microdomains, T_{ODT} showed a slight depression. SBR25 dissolves mostly into the PB microdomain of S–B50 to increase lamella microdomain spacing; thus its addition makes the overall composition of S and B in the mixture more asymmetrical. On the other hand, when SBR having nearly symmetric composition (SBR50 and SBR60) is added to S–B50, T_{ODT} decreases heavily because SBR acts as neutral solvent. SBR50 or SBR60 is not completely homogeneously mixed as dilution approximation assumes, but might be localized into the S–B50 microdomain interface. Therefore, extension between junction points results in the contraction of measured lamella microdomain spacing.

Above the solubility limit of SBR, where macroscopic

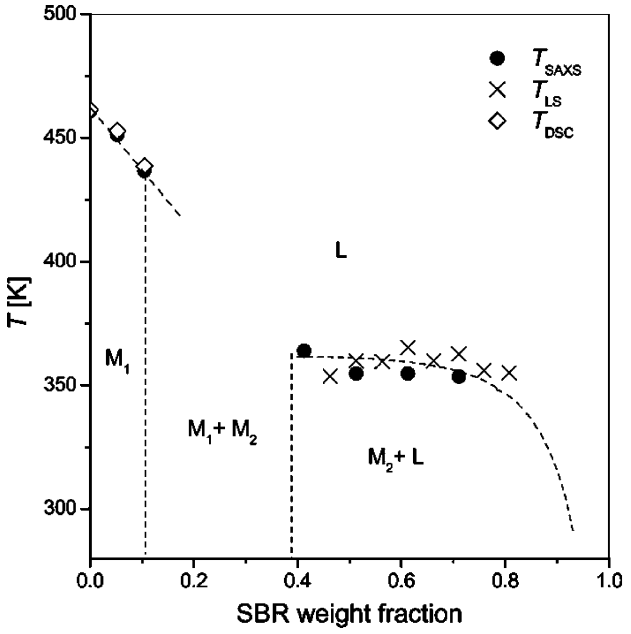

Fig. 10. Phase diagram obtained from SAXS, DSC, and LS studies for S–B50/SBR25. Listed symbols are T_{SAXS} (●), T_{LS} (×), and T_{DSC} (◇). The dashed line denotes the phase boundary drawn as a guide to the eye.

phase separation occurs, the depression of T_{ODT} behaves like a melting point depression. The phase diagrams for S–B containing symmetric SBR show three regions: two homogeneous phases, 'M' and 'L', and one region of two-phase coexistence, 'M+L'. The 'M+L' phase below the transition line which indicates that the ordered 'M' phase rich in S–B50 and the disordered 'L' phase rich in SBR coexist in a macroscopically phase-separated state. The phase diagram for S–B containing asymmetric SBR shows a succession of mixed mesophases of different morphologies from lamellae and cylindrical to disordered liquid phases. Many of the results obtained in this study can be explained and rationalized on the basis of the phase diagram shown in Fig. 8 and Fig. 10. The data obtained here are, however, not sufficient by themselves to allow construction of phase diagrams in accurate detail. Collection of much more comprehensive sets of data is required for this purpose.

Acknowledgements

This work was supported by the Center for Advanced Functional Polymers. The authors are grateful to the Pohang Accelerator Laboratory in performing SAXS measurements.

References

[1] Zin WC, Roe RJ. Macromolecules 1984;17:183.
[2] Roe RJ, Zin WC. Macromolecules 1984;17:189.
[3] Kang CK, Zin WC. Macromolecules 1992;25:3039.
[4] Matsen MW. Macromolecules 1995;28:5765.
[5] Whitmore MD, Noolandi J. Macromolecules 1985;18:2846.
[6] Winey KI, Thomas EL, Fetters LJ. Macromolecules 1991;24:6182.
[7] Nojima S, Roe RJ. Macromolecules 1987;20:1866.
[8] Tanaka H, Hasegawa H, Hashimoto T. Macromolecules 1991;24:240.
[9] Baek DM, Han CD, Kim JK. Polymer 1992;33:4821.
[10] Tucker PS, Barlow JW, Paul DR. Macromolecules 1988;21:1678.
[11] Tucker PS, Barlow JW, Paul DR. Macromolecules 1988;21:2794.
[12] Tucker PS, Paul DR. Macromolecules 1988;21:2801.
[13] Hashimoto T, Kimishima T, Hasegawa H. Macromolecules 1991;24:5704.
[14] Lee HK, Kang CK, Zin WC. Polymer 1996;37:287.
[15] Tanaka H, Hashimoto T. Macromolecules 1991;24:5713.
[16] Cifra P, Karasz FE, MacKnight WJ. Macromolecules 1989;22:3649.
[17] Shi AC, Noolandi J, Hoffmann H. Macromolecules 1994;27:6661.
[18] Lee HK, Zin WC. Macromolecules 2000;33:2894.
[19] Kim DC, Lee HK, Sohn BH, Zin WC. Macromolecules 2001;34:7767.
[20] Lee HK, Kim DC, Yoo SI, Sohn BH, Zin WC. Macromolecules 2003;36:7740.
[21] Hong KM, Noolandi J. Macromolecules 1983;16:1083.
[22] Fredrickson GH, Leibler L. Macromolecules 1989;22:1238.
[23] de la Cruz MO. J Chem Phys 1989;90:1995.
[24] Lodge TP, Hamersky MW, Hanley KJ, Huang CI. Macromolecules 1997;30:6139.
[25] Lodge TP, Pudil B, Hanley KJ. Macromolecules 2002;35:4707.
[26] Whitmore MD, Noolandi J. J Chem Phys 1990;93:2946.
[27] Stühn B, Mütter R, Albrecht T. Europhys Lett 1992;18:427.
[28] Bates FS. Macromolecules 1985;18:525.
[29] Guenza M, Schweizer KS. J Chem Phys 1997;106:7391.
[30] Fredrickson GH, Helfand E. J Chem Phys 1987;87:697.
[31] Matsushita Y, Torikai N, Mogi Y, Noda I, Han CC. Macromolecules 1993;26:6346.